Synergistic effects of zinc oxide in montmorillonite flame-retardant polystyrene nanocomposites

Yongqin Han, Tingxi Li, Bo Gao, Li Gao, Xiujuan Tian, Qiang Zhang, Yanmin Wang

Department of Polymer Material, College of Materials Science and Engineering, Shandong University of Science and Technology, Qingdao 266510, People's Republic of China
Correspondence to: Y. Han (E-mail: yongqinhan@126.com)

ABSTRACT: In this study, two-dimensional organic montmorillonite (OMMT) and one-dimensional needlelike ZnO were used as flame retardants of polystyrene (PS). Polystyrene/organic montmorillonite (PMT) and polystyrene/organic montmorillonite/zinc oxide nanocomposites (PMZs) with different weight ratios were prepared by melt intercalation. Information on the morphologies and structures of the PS nanocomposites was obtained with Fourier transform infrared spectroscopy, X-ray diffraction, scanning electron microscopy, and transmission electron microscopy. The results indicate that a mixed exfoliated–intercalated structure was observed in the PMT and PMZs. Dynamic mechanical thermal analysis showed that both the storage modulus and glass-transition temperature values of the PMT and PMZs were significantly improved compared with those of the neat PS. The mechanical property tests showed that the bending modulus values of both PM5 (PS/OMMT weight ratio = 95:5) and PMZs increased compared with that of pristine PS. PMZ1 (PS/OMMT/ZnO weight ratio = 94:5:1) provided no decrease in the tensile strength in comparison with PS. A synergistic effect was observed between OMMT and ZnO; this resulted in improvements in the flame retardancy and dynamic mechanical properties in the PMZs. © 2015 Wiley Periodicals, Inc. J. Appl. Polym. Sci. **2016**, *133*, 43047.

INTRODUCTION

Polystyrene (PS) is one of the most widely used plastics because of its affordability, light density, excellent mechanical durability, and convenience of processing and molding. With advancements in technology, the rate of consumption of PS in households, laboratories, and businesses is continually increasing. PS is used heavily as a building insulation material, in architectural models, and as a packing material for food, laboratory chemicals, and electronic appliances. However, its high flammability and severe dripping during combustion greatly limit its applications in such areas. To solve this problem, halogen-containing and halogen-free flame retardants have been used to obtain flame-retardant PS. Generally, halogen-containing fire retardants are considered effective. However, their potential to corrode metal components and, more pressingly, the toxicity of the hydrogen halide formed during combustion are obvious disadvantages. There has been increasing interest in the use of halogen-free flame-retardant substances. In recent years, many more efforts have been made to use inorganic nanofillers, such as montmorillonite (MMT),[1–6] layered hydrogen oxides,[7–10] carbon nanotubes,[11–13] and graphene,[14–17] for flame retardants.

Among nanofillers, clay and layered hydrogen oxides are the most widely used for preparing polymer nanocomposites because these compounds are easily available and well characterized. MMT is a crystalline 2:1 layered clay mineral in which a central alumina octahedral sheet is sandwiched between two silica tetrahedral sheets.[18] MMT can act as a barrier to oxygen and flammable materials.[18,19] Polymer/montmorillonite nanocomposites (PMNs) have drawn a great deal of interest from academic and industrial researchers because of their outstanding combination properties, for instance, their improved mechanical properties, a remarkable increase in the thermal stability, their flame retardancy, and a reduction in the permeability of gases. Several mechanisms have been proposed to explain the flame retardancy of PMNs. Until now, the general view of the flame-retardant mechanism is that a carbonaceous silicate char is produced on the surface of the nanocomposite during burning; this creates a protection barrier against heat and mass transfer.[20–22] It has been reported that high amounts of MMT particles (>5 wt %) might be agglomerated into larger MMT particles in the polymer matrix, and this causes the poor dispersion of MMT particles in the polymer matrix. This also reduces the interaction effect in the polymer matrix and, thus, ruins the performances of the polymers, such as the mechanical and flame-retardant performances.[23–25]

ZnO is an inorganic filler and semiconductor material existing in a diversity of structures. It is also an inorganic UV absorber having a

Table I. Temperature Profile along the Extruder

	Zone 1	Zone 2	Zone 3	Zone 4	Zone 5	Die
Temperature (°C)	180	200	205	200	205	195

wide band-gap energy that is used as a UV stabilizer in organic coatings.[26,27] When used as a nanoparticle, it provides a combination of more efficient UV absorption and high visible transparency when it is dispersed in a thin film. Nano-ZnO was investigated as a UV absorber in a polyurethane/acrylic clear topcoat.[26] ZnO addition to a polymer material increased the mechanical properties and thermal stability of composite materials.[28] Recently, the synergistic effects of ZnO with intumescent flame retardant in a flame-retardant silicone rubber system were reported.[29] It proved that the addition of ZnO was capable of initiating a compact and homogeneous char on the surface; this turned out to be of most importance for the flame-retardant performance. To our best knowledge, however, few research studies on the synergistic effects of ZnO with MMT flame-retardant PS systems have been reported. In this study, flame-retardant PS nanocomposites were prepared with MMT as the flame retardant and microneedlelike ZnO as a synergistic agent. The effects of the MMT/ZnO composite system on the thermal stability, flame retardancy, and dynamic mechanical properties were investigated. The PS/organic montmorillonite (OMMT) and polystyrene/organic montmorillonite/zinc oxide nanocomposites (PMZs) prepared in this study could be used as potential materials in construction materials and electronic parts because of their good flame retardancy and mechanical properties.

EXPERIMENTAL

Materials
The clay used in this study as a host material was sodium OMMT (1000 mesh); it was supplied by the Chinese Academy of Sciences (Peking, China). OMMT was prepared by an ion-exchanging reaction between sodium MMT and octadecyl ammonium (ODA) salt.[30] The presence of ODA cations in the galleries provided hydrophobicity for the sodium MMT. Needlelike ZnO was purchased from Hefei Ai Jia New Materials Technical Co. with a length size of 10–100 μm. General PS resin (PG-383) was purchased from Taiwan Chi Mei Industrial Factory.

Preparation of the Polystyrene/Organic Montmorillonite (PMT) and PMZs
The PMT composite samples were obtained by melt mixing. Given amounts of OMMT and ZnO were mixed evenly with PS; then, the mixture was put into a twin-screw extruder for further melt blending in the temperature range 180–205°C and a screw speed of 200 rpm. The temperature profile along the extruder is listed in Table I. Finally, the strands obtained from the extruder were cut into small granules in a granulator. The MMT/ZnO/PS weight ratio is illustrated in Table II. The prepared nanocomposites were named PM5, PMZ0.5, PMZ1, PMZ2, and PMZ5, respectively. Sample bars suitable for cone calorimetry testing and dynamic mechanical thermal analysis (DMTA) were prepared via compression molding at a processing temperature of 180°C.

Characterization

Fourier Transform Infrared (FTIR) Spectroscopy. Samples for the FTIR measurements were mixed with KBr powder and pressed into a tablet. The FTIR spectra were obtained with a Bruker Vector22 FTIR spectrophotometer in the range 400–4000 cm^{-1}.

Scanning Electron Microscopy (SEM). The SEM images were obtained on a Hitachi S-4800 scanning electron microscope. SEM images were obtained on freeze-fractured cross sections of the PS composite sample bars.

Transmission Electron Microscopy (TEM). The TEM micrographs shown in this article were obtained with a JEOL JEM-2100 electron microscope operated at 200 kV. To reveal the microstructure of the PS nanocomposites under TEM, ultrathin films (ca. 50 nm) were prepared by the sectioning of the samples at room temperature with an Ultracut UC7 microtome (Leica, Germany) with a diamond knife.

X-ray Diffraction (XRD). XRD patterns were obtained with a D/Max2500PC X-ray diffractometer with Cu Kα radiation ($\lambda = 0.1541$ nm).

Thermogravimetric Analysis (TGA). TGA was carried out in air at a heating rate of 10°C/min with a Netzsch STA409 PC thermoanalyzer instrument.

Dynamic Mechanical Analysis (DMA). Dynamic mechanical properties were measured with a DMA/SDTA861e (Mettle, Switzerland) in stretching mode on sample bars (9 × 4 × 0.4 mm^3). A temperature ramp experiment (2°C/min) was conducted under air from room temperature to 180°C at a constant frequency of 1 Hz.

Mechanical Properties. Tensile and flexural tests were conducted at room temperature with an electronic universal testing instrument (TCS-2000, Gotech Testing Machine Co., Ltd., Dongguan, China) according to ASTM D 638 and ASTM 790, respectively. All of the material types were evaluated five times to reduce the experimental error.

Limited Oxygen Index (LOI). The LOI values were measured on an HC-2C oxygen index meter (Jiangning, China) according to ASTM D 2863, and the dimensions of all of the samples were 130 × 6.5 × 3.0 mm^3.

Cone Calorimetry Testing. The combustion properties of the PMT nanocomposites were evaluated with a cone calorimetry experiment. All of the samples (100 × 100 × 3 mm^3) were exposed to a FTT 0007 cone calorimeter (FTT Co., England)

Table II. Weight Ratios of the MMT–ZnO–PS Samples

Sample ID	PS (%)	MMT (%)	ZnO (%)
PS	100	0	0
PM5	95	5	0
PMZ0.5	94.5	5	0.5
PMZ1	94	5	1
PMZ2	93	5	2
PMZ5	90	5	5
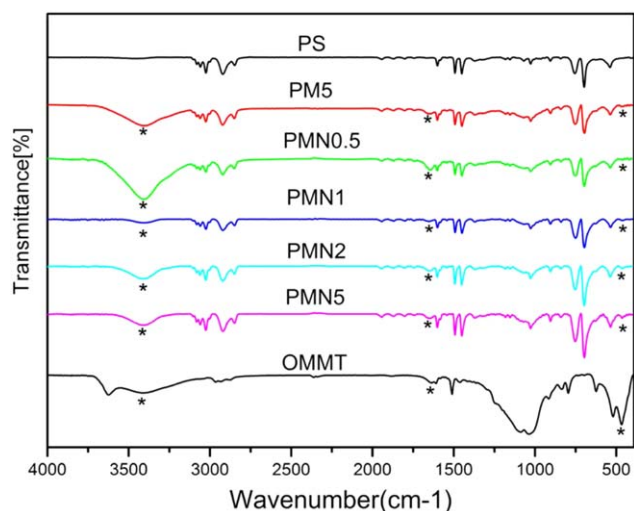
Figure 1. FTIR spectra of PS, PM5, PMZ0.5, PMZ1, PMZ2, and PMZ5. [Color figure can be viewed in the online issue, which is available at wileyonlinelibrary.com.]

under a heat flux of 50 kW/m^2 according to ISO-5660 standard procedures.

RESULTS AND DISCUSSION

Structure and Morphology

Figure 1 shows the FTIR spectra of the PS and its nanocomposites. As shown in the FTIR spectrum of the pure PS, the bands in the region 3000–3100 cm^{-1} were attributed to ═C─H aromatic stretching vibrations. The peaks at 2920 and 2849 cm^{-1} represented the asymmetric and symmetric stretching vibrations of CH$_2$, respectively. The bands centered at 1600, 1580, and 1491 cm^{-1} were due to the stretching vibrations of benzene ring, and the peaks at 753 and 697 cm^{-1} were related to the C─H out-of-plane bending vibrations of the benzene ring.[31] In the spectrum of OMMT, the bands in the region 2800–3000 cm^{-1} and centered at about 1470 cm^{-1} were attributed to the CH$_2$ vibrations of the ODA salt.[32] The broad doublet bands near 1038 and 1089 cm^{-1} were assigned as the characteristic absorption of OMMT for Si─O stretching vibrations in the tetrahedral sheet. The bands centered at 519 and 467 cm^{-1} were attributed to Si─O bending vibrations due to Si─O─Al and Si─O─Si, respectively.[33] Moreover, the band centered at 3628 cm^{-1} was ascribed to O─H stretching of lattice water in OMMT. The stretching and deformation bands of ─OH on the OMMT layer were centered around 3410 and 1645 cm^{-1}. In a comparison with the spectra of PS and OMMT, characteristic bands of PS and some peaks of OMMT (marked by asterisks) and Zn─O skeleton (marked by triangles) were found in the PMT and PMZs.

Figure 2 shows the XRD patterns of OMMT, needlelike ZnO, PS, and the nanocomposites. A strong diffraction peak around a 2θ of 5.88° was displayed for OMMT; this was equal to a d-spacing of 1.50 nm for the layered silicates in OMMT. The XRD patterns of ZnO showed that needlelike ZnO had good crystallinity. The characteristic peak of (100), (002), (101), (102), (110), (103), and (112) were in agreement with those of

the standard of standard patterns of hexagonal wurtzite ZnO (JCPDS 36-1451).[34–36] Only two peaks centered at 2θ values of 5.88 and 29° with weak intensities were observed in the PMT nanocomposites; this suggested the formation of a mixed exfoliated/intercalated structure. The (100), (101), (102), and (110) basal planes of ZnO were found in the nanocomposites of PMZ; this indicated the incorporation of ZnO in the PMT nanocomposites. Furthermore, the irregular diffraction peaks in the nanocomposites were attributed to the disturbed orientation of clay layers because of exfoliation. PMZs, including PMZ0.5, PMZ1, PMZ2, and PMZ5, showed a gradual increasing intensity of these diffraction peaks; this was attributed to the increasing content of ZnO.

SEM photographs of OMMT and ZnO are shown in Figure 3. We observed from Figure 3(a) that OMMT provided an overlapped layered structure. ZnO showed a needlelike morphology with an average diameter that varied from 5 to 10 μm and a length size of 30–80 μm. SEM micrographs of the fractured surfaces of the PMT and PMZs are shown in Figure 4. Exfoliated and a few overlapped layers of OMMT in the PS nanocomposites were observed. For PMZ1, it was hard to distinguish OMMT and ZnO from the PS matrix, probably because of the uniform distribution of both OMMT and ZnO in the PS nanocomposites. Compared with the other PMZs, PMZ5 provided a rather rougher surface, probably because of the high content of ZnO in the nanocomposites.

The nanocomposites were also characterized by TEM (Figure 5) to study the distribution of OMMT and ZnO. Figure 5(a) shows that PM5 (PS/OMMT weight ratio = 95:5) presented an intercalated nanomorphology with many exfoliated layers in the polymer matrix; this was consistent with the XRD results. As shown in Figure 5(b–e), a nanostructure with a higher degree of intercalation was observed when a more needlelike ZnO was introduced.

Mechanical Properties

Mechanical reinforcement is also reflected in the dynamic mechanical properties. DMA is used to measure the response of
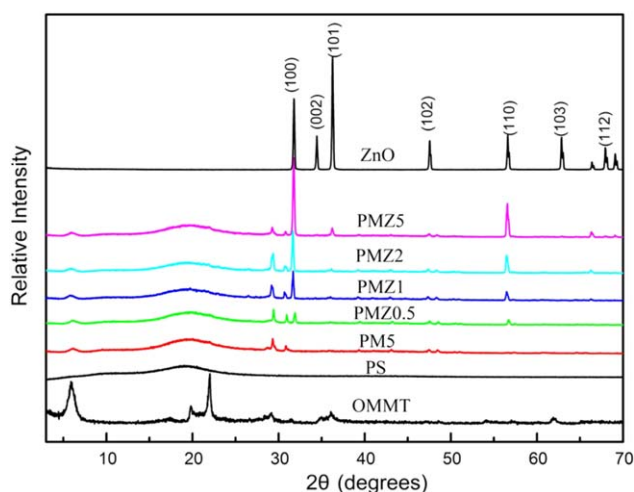
Figure 2. XRD patterns of OMMT, PM5, PMZ0.5, PMZ1, PMZ2, PMZ5, and ZnO. [Color figure can be viewed in the online issue, which is available at wileyonlinelibrary.com.]
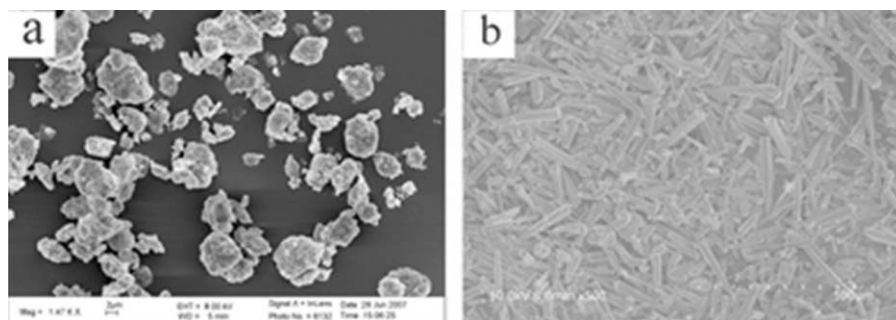
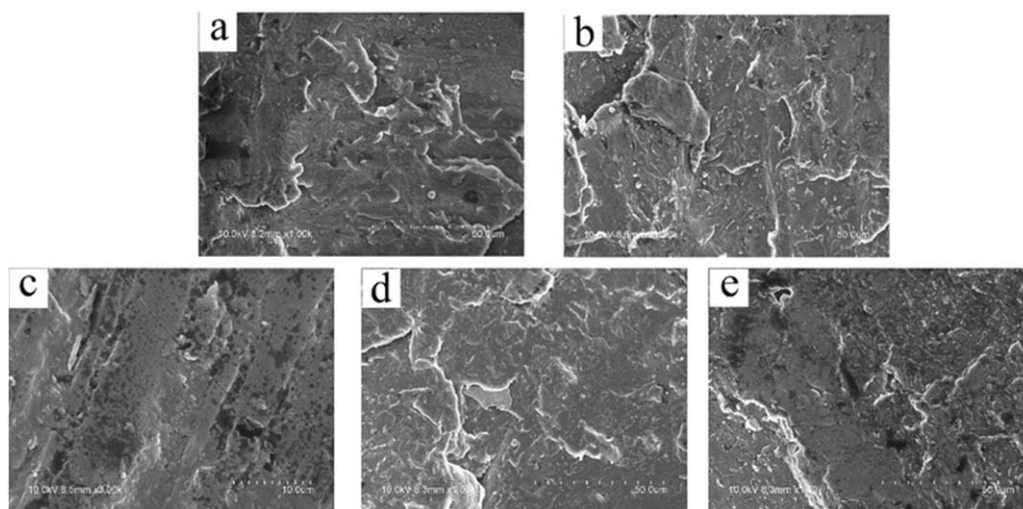**Figure 3.** SEM photos of (a) OMMT and (b) ZnO.

Figure 4. SEM photos of (a) PM5, (b) PMZ0.5, (c) PMZ1, (d) PMZ2, and (e) PMZ5.

a material to cyclic deformation. The three main properties typically determined are the storage modulus (E') corresponding to the elastic response to deformation, the loss modulus describing the plastic response to the deformation, and their ratio, tan δ. At various temperatures, these properties are related to transitions involving polymer mobility or segmental dynamics within the sample, such as the glass transition.

As shown in Figure 6, a significant increase in E' was observed. In both glassy and rubbery regions, the E' values of the PMT and PMZs were higher than that of pure PS. The measurement of E' at different temperatures and the data obtained from the tan δ plot are summarized in Table III. The addition of 5.0 wt % OMMT produced a significant increase to 100.1% (from 1.5 to 3.1 GPa) in E' in the glassy state (at 27°C, where the
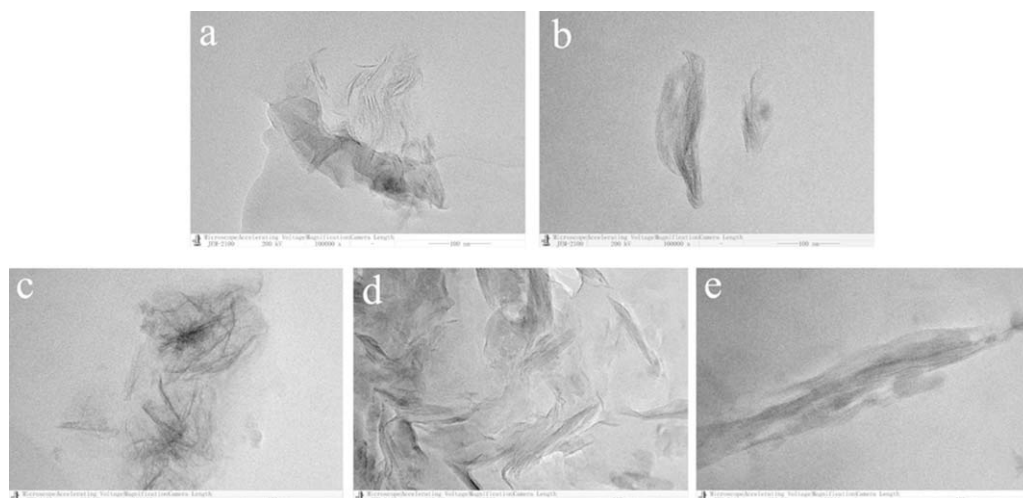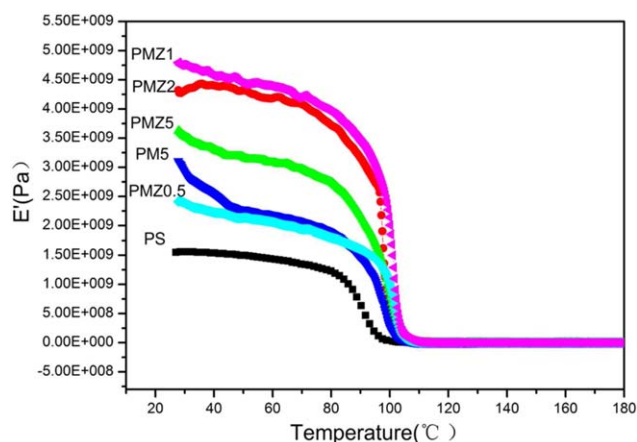

**Figure 5.** TEM images of (a) PS, (b) PM5, (c) PMZ0.5, (d) PMZ1, and (e) PMZ2.

Figure 6. E′ values for PS, PM5, PMZ0.5, PMZ1, PMZ2, and PMZ5 at a frequency of 1 Hz at various temperatures. [Color figure can be viewed in the online issue, which is available at wileyonlinelibrary.com.]

molecules were frozen). The significantly improved modulus was attributed to the OMMT layer reinforcement, the improved interfacial interaction, and the mobility restriction of the polymer chains.[37–39] It was interesting that the further addition of needlelike ZnO first produced a small decrease in E′ and then a significant increase when the ZnO content reached 1 wt % compared with PMT5. Unfortunately, further increases in the ZnO content led to a decrease in E′ because E′ is mainly related to the structural network created between OMMT, ZnO, and macromolecular chains. The incorporation of a small amount of ZnO (1 wt %) increased the polymer/OMMT interactions. The two-dimensional OMMT layer, together with one-dimensional ZnO needles, acted as physical crosslinks (as shown in Figure 7); this limited the movements of the macromolecular chains of PS during glass transition. The physical crosslink might have been disturbed as the ZnO content increased further. As a result, the E′ values of PMZ2 and PMZ5 decreased compared with that of PMZ1.

Figure 8 shows the loss factor curves of the pure PS and its nanocomposites. The temperature at which the curve showed a maximum peak was recorded as the glass-transition temperature (T_g). The T_g values for the PM0.5 and PMZs increased significantly as compared with that of pure PS. The T_g values of the nanocomposites were 14–19°C higher than that of the neat PS.

**Table III.** E′ and T_g Values of the Nanocomposites Obtained from DMTA

Sample	E′ (MPa)		T_g (°C)
	At 50°C	At 100°C	
PS	1500	256	101
PM5	2279	255	115
PMZ0.5	2132	1015	116
PMZ1	4435	2005	120
PMZ2	4318	466	116
PMZ5	3173	775	118
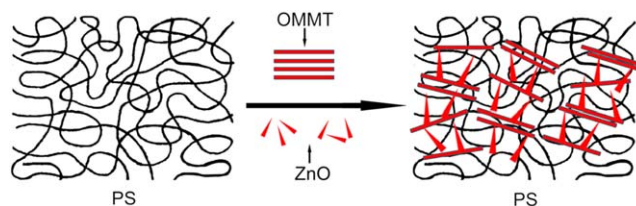
Figure 7. Schematic representation of the formation of the physical cross-link structure in the PMZs. [Color figure can be viewed in the online issue, which is available at wileyonlinelibrary.com.]

The good dispersion of OMMT layers and needlelike ZnO in the nanocomposites facilitated enhanced interfacial interaction between the sheet and polymer matrix and, thus, significantly restricted the segmental movement of the polymer chains.[38] This led to a higher T_g shift.

The effects of OMMT and ZnO on the mechanical properties of the PS composites were studied, with the results summarized in Table IV. We observed that the bending moduli of both PM5 and PMZs increased compared with that of pristine PS. Unfortunately, the incorporation of 5 wt % OMMT resulted in a 25.1% decrease in the tensile strength. When the combination of ZnO with OMMT was applied, a further decrease in the tensile strength of the PS composites was observed. It was interesting that when 5 wt % OMMT and 1 wt % ZnO were added, the tensile strength of PMZ1 increased back to 49.5 MPa. Further increase in ZnO led to a decrease of about 10% in the tensile strength compared with pristine PS. It is also shown in Table IV that the incorporation of OMMT decreased both the elongation at break and the bending strength of PS. The value of the elongation at break and bending strength of PMZ1 reached maximum values of 8.6% and 85.8 MPa, respectively, for PMZs. Such an enhancement compared with PM5 could also be attributed to the three-dimensional physical network structure constructed by the two-dimensional OMMMT and one-dimensional ZnO (see Figure 7).
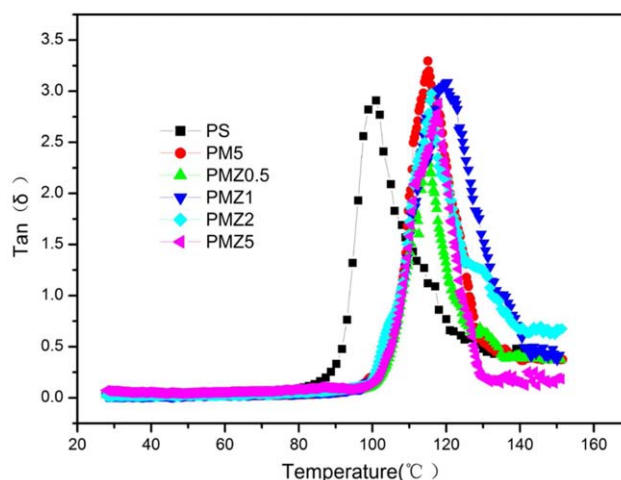
Figure 8. Tan δ curves for PS, PM5, PMZ0.5, PMZ1, PMZ2, and PMZ5 at a frequency of 1 Hz at various temperatures. [Color figure can be viewed in the online issue, which is available at wileyonlinelibrary.com.]

Table IV. Mechanical Properties of the PS, PM5, and PMZs

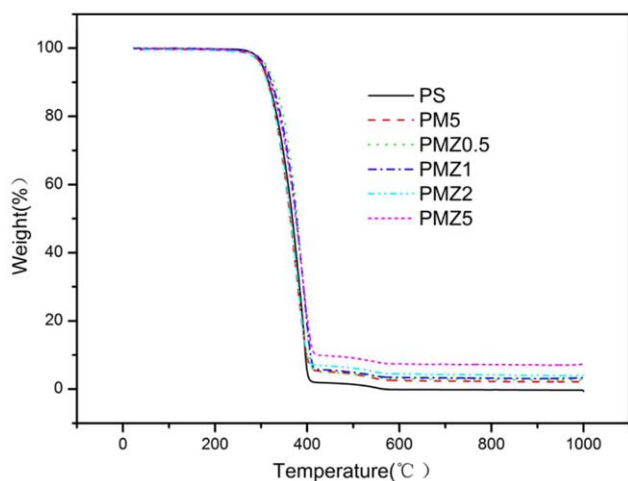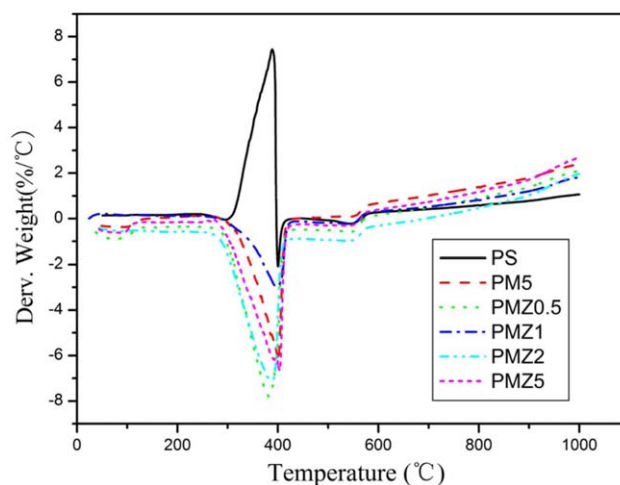| Sample	Tensile strength (MPa)	Elongation at break (%)	Bending strength (MPa)	Bending modulus (MPa)
PS	49.4	9.4	89.6	2990.1
PM5	37.0	7.1	75.5	3175.2
PMZ0.5	28.8	6.8	79.2	3377.0
PMZ1	49.5	8.6	85.8	3370.8
PMZ2	44.4	7.0	68.8	3083.9
PMZ5	44.0	7.6	68.1	3098.0

Thermal Properties

The TGA and derivative thermogravimetry (DTG) curves of the neat PS and its nanocomposites in air are shown in Figures 9 and 10. The relevant thermal decomposition data are listed in Table V; these include the temperature at which 5% weight loss occurred (T_{onset}), the temperature at the maximum weight loss rate (T_{max}), and the char residues at 1000°C. Figure 9 shows that T_{onset} of the neat PS was 302°C, and T_{max} was 399°C under a nitrogen atmosphere. The addition of OMMT increased T_{onset} and T_{max} of PM5. However, the further addition of needlelike ZnO slightly decreased T_{onset} and T_{max}. This was attributed to the increased degree of intercalation nanostructure of the nanocomposites caused by needlelike ZnO. We observed that compared with PMZ0.5 and PMZ2, PMZ1 and PMZ5 had better thermal stability. We also noted that the composites yielded much more char residues; this could be beneficial for the improvement of the flame retardancy of PS. The PM5 and PMZ residual solids at 1000°C were from 2.2 to 8.3%. The increased amount of residue may have been due to the formation of more thermally stable carbonaceous char[39] and the presence of MMT and ZnO.

Flame-Retardant Properties

The flame-retardant properties of the PMT and PMZs were evaluated by cone calorimetry. A cone calorimeter is an effective

Figure 10. DTG curves of PS, PM5, PMZ0.5, PMZ1, PMZ2, and PMZ5. [Color figure can be viewed in the online issue, which is available at wileyonlinelibrary.com.]

Table V. TGA and DTG Data of PS, PM5, and PMZs

Sample	Weight loss temperature (°C)		1000°C char (%)
	T_{onset}	T_{max}	
PS	302	399	0
PM5	311	401	2.2
PMZ0.5	301	382	2.8
PMZ1	308	398	3.2
PMZ2	299	388	3.9
PMZ5	305	405	8.3

bench-scale apparatus for simulating real fire scenarios. The most important parameter obtained by cone calorimetry measurements is the heat-release rate (HRR), especially its peak

Figure 9. TGA curves of PS, PM5, PMZ0.5, PMZ1, PMZ2, and PMZ5. [Color figure can be viewed in the online issue, which is available at wileyonlinelibrary.com.]
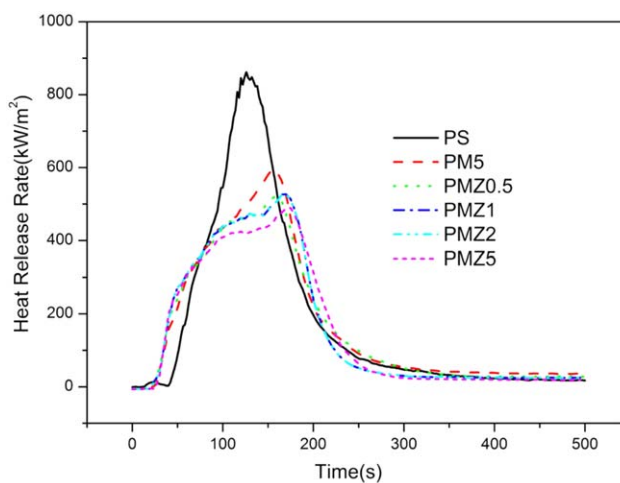

Figure 11. HRR versus burning time for PS, PM5, PMZ0.5, PMZ1, PMZ2, and PMZ5. [Color figure can be viewed in the online issue, which is available at wileyonlinelibrary.com.]

**Table VI.** PHRR and LOI Values of PS, PM5, and PMZs

Sample	PHRR (kW/m^2)	LOI (%)
PS	861	17.4
PM5	359	19.8
PMZ0.5	316	20.2
PMZ1	317	20.5
PMZ2	317	20.2
PMZ5	295	20.9

heat-release rate (PHRR), which can be viewed as the driving force of the fire. Detailed data from the cone calorimeter are reported in Figure 11 and Table VI. We observed that the pure PS burned fast after ignition, and a sharp HRR appeared, with a PHRR of 861 kW/m^2. For PM5, shown in Figure 11, PHRR decreased from 861 to 359 kW/m^2 (a 58% reduction). The further addition of ZnO led to about a 63–66% reduction in PHRR. These results indicate that a combination effect of OMMT and ZnO improved the flammability properties of the PS nanocomposites.

The LOI values of PS, PM5, and PMZs are shown in Table VI. Neat PS is a highly flammable thermoplastic with a very low LOI value (17.4%). We observed that the addition of OMMT improved the LOI of the nanocomposite to some extent. The LOI value of the PMZs increased slightly with further addition of ZnO. Compared with the decrease in the PHRR value, the effect of inorganic fillers on the LOI values was not significant.[25]

To further study the role of OMMT and ZnO in the combustion of the PS nanocomposites, the morphologies of the chars after combustion were investigated with a digital camera after cone calorimetry tests. Figure 12 shows the digital photos for the residues of PS, PM5, and PMZs. As shown in Figure 10(a), almost no residue was observed after PS burned. From the pictures, we found that more combustion residues of PMZs were obtained than those of PM5; this was in good accordance with the char yields obtained by the TGA results. This result suggests that the OMMT–ZnO system effectively improved the charring properties of the PS nanocomposites. Moreover, a lot of multilayered bulks appeared on the charred layers of the PMZs. The multilayered layers of PMZ5 were quite intact. This result evidently demonstrated that the charred layers of PM5 became firm with the addition of ZnO.

It has been reported that the flame-retardant mechanism of PMT nanocomposites is closely associated with the diffusion of volatile decomposed products and heat transfer in the condensed phase. The charring behavior plays a vital role in determining the fire performance of the nanocomposite.[40] The char covered on the polymer surface resists the heat transfer to the inner region to vaporize the flammable polymer volatiles and prevent them from supplying fuel for the combustion process. Thus, this could further retard the combustion of the polymer matrix. Needlelike ZnO had a large surface area and low density and tended to migrate near the regressing sample surface without sinking through the polymer melt during the gasification/burning process.[25] The physical crosslinking networks constituted by layered OMMT and ZnO needles consequently
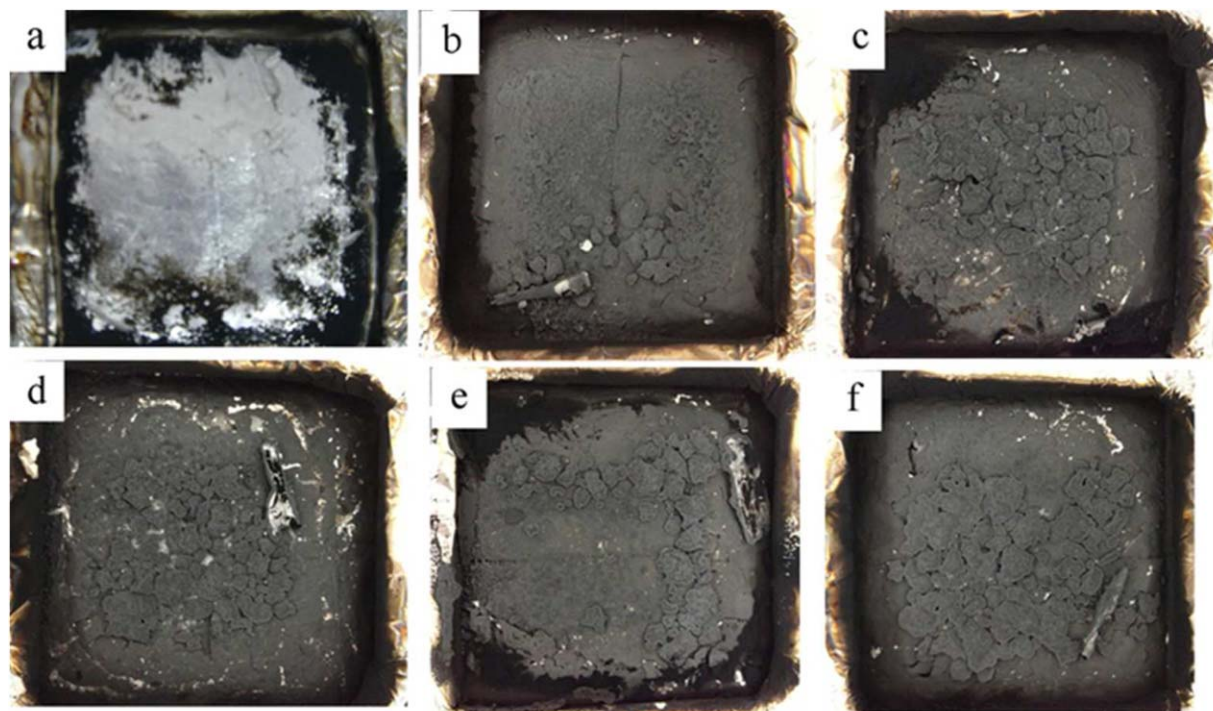
Figure 12. Residues at the end of the cone calorimetry tests: (a) PS, (b) PM5, (c) PMZ0.5, (d) PMZ1, (e) PMZ2, and (f) PMZ5. [Color figure can be viewed in the online issue, which is available at wileyonlinelibrary.com.]

formed a multilayered charred layer, which acted as a heat-insulation barrier. This charred layer prevented heat transfer and the transportation of degraded products between the melting polymer and the surface; this further reduced the HRR values.

CONCLUSIONS

PMT and PMZ nanocomposites were prepared by the melt blending of PS with OMMT and ZnO. The results from XRD and TEM show that the PM5 and PMZs showed a mixed exfoliated/interacted structure. The DMTA results show that both E' and T_g of the PM and PMZs were significantly improved compared with those of neat PS. The T_g values of the nanocomposites were 14–19°C higher than that of the neat PS. The addition of 5.0 wt % OMMT produced a significant increase to 100.1% (from 1.5 to 3.1 GPa) in E'. Among the PMZs, PMZ1 showed a maximum E' of 4.4 GPa; this was 185.8% higher than that of neat PS. The bending modulus of both the PM5 and PMZs increased compared with that of the pristine PS. PMZ1 provided no decrease in the tensile strength in comparison with PS. The calorimetry tests results show that the combination effect of OMMT and the needlelike ZnO improved the flame-retardant performance of PS. PHRR decreased from 861 to 359 kW/m^2 (a 58% reduction) for PM5. A further addition of ZnO led to about a 63–66% reduction in PHRR. The physical crosslinking networks constituted by layered OMMT and ZnO needles consequently formed a multilayered charred layer, which acted as a heat-insulation barrier.

ACKNOWLEDGMENTS

REFERENCES

1. Zhong, Y. H.; Wu, W.; Lin, X. Q.; Li, M. L. *J. Appl. Polym. Sci.* **2014**, *131*, 41094.

2. Zhang, X. J.; Ren, F.; Zhang, L. Q.; Dong, D. W.; Jiang, K.; Lu, Y. L. *J. Appl. Polym. Sci.* **2014**, *131*, 40972.

3. Wang, J. N.; Su, X. Y.; Mao, Z. P. *Polym. Degrad. Stab.* **2014**, *109*, 154.

4. Zhang, R. C.; Hong, S. M.; Koo, C. M. *J. Appl. Polym. Sci.* **2014**, *131*, 40648.

5. Ramani, A.; Dahoe, A. E. *Polym. Degrad. Stab.* **2014**, *105*, 1.

6. Wang, J. N.; Mao, Z. P. *J. Appl. Polym. Sci.* **2014**, *131*, 39625.

7. Gao, Y. S.; Wang, Q.; Wang, J.; Huang, L.; Yan, X.; Zhang, X.; He, Q.; Xing, Z.; Guo, Z. *Am. Chem. Soc. Appl. Mater. Interface* **2011**, *6*, 5094.

8. Hong, N. N.; Song, L.; Wang, B. B.; Stec, A. A.; Hull, T. R.; Zhan, J.; Hu, Y. *Mater. Res. Bull.* **2014**, *49*, 657.

9. Liu, X. S.; Gu, X. Y.; Zhang, S.; Jiang, Y.; Sun, J.; Dong, M. Z. *J. Appl. Polym. Sci.* **2013**, *5*, 3645.

10. Huang, G. B.; Chen, S. Q.; Song, P. G.; Lu, P. P.; Wu, C. L.; Liang, H. D. *Appl. Clay Sci.* **2014**, *88–89*, 78.

11. Yu, T.; Jiang, N.; Li, Y. *Compos. Sci. Technol.* **2014**, *104*, 26.

12. Pandey, P.; Mohanty, S.; Nayak, S. K. *High Perform. Polym.* **2014**, *26*, 826.

13. Zhang, Z. Y.; Yuan, L.; Liang, G. Z.; Gu, A. J.; Qiang, Z. X.; Yang, C. W.; Chen, X. X. *J. Mater. Chem. A* **2014**, *2*, 4975.

14. Yu, B.; Shi, B. H.; Qiu, S. L.; Xing, W. Y.; Hu, W. Z.; Song, L.; Lo, S. M.; Hu, Y. *J. Mater. Chem. A* **2015**, *3*, 8034.

15. Dittrich, B.; Wartig, K. A.; Muelhaupt, R.; Schartel, B. *Polymer* **2014**, *6*, 2875.

16. Ran, S. Y.; Chen, C.; Guo, Z. H.; Fang, Z. P. *J. Appl. Polym. Sci.* **2014**, *131*, 40520.

17. Han, Y. Q.; Wu, Y.; Shen, M. X.; Huang, X. L.; Zhu, J. J.; Zhang, X. G. *J. Mater. Sci.* **2013**, *48*, 4214.

18. Zanetti, M.; Costa, L. *Polymer* **2004**, *45*, 4367.

19. Park, K. W.; Kwon, O. Y. *J. Ind. Eng. Chem.* **2004**, *10*, 252.

20. Kashiwagi, T.; Harris, R. H., Jr.; Zhang, X.; Briber, R. M.; Cipriano, B. H.; Raghavan, S. R.; Awad, W. H.; Shields, J. R. *Polymer* **2004**, *45*, 881.

21. Gilman, J. W.; Harris, R. H., Jr.; Shields, J. R.; Kashiwagi, T.; Morgan, A. B. *Polymer. Adv. Tech.* **2006**, *17*, 263.

22. Gilman, J. W.; Kashiagi, T. In Polymer–Clay Nanocomposites; Pinnavaia, T. J., Beall, G. W., Eds.; Wiley: New York, **2000**; p 193.

23. Bee, S. T.; Hassan, A.; Ratnam, C. T.; Tee, T. T.; Sin, L. T.; Hui, D. *Compos. B* **2014**, *61*, 41.

24. Sanchez-Olivares, G.; Sanchez-Solis, A.; Calderas, F.; Medina-Torres, L.; Manero, O.; Di Blasio, A.; Alongi, J. *Appl. Clay Sci.* **2014**, *102*, 254.

25. Liu, J. C.; Fu, M. Y.; Jing, M. M.; Li, Q. Y. *Polym. Adv. Technol.* **2013**, *24*, 273.

26. Lowry, M. S.; Hubble, D. R.; Wressell, A. L.; Vratsanos, M. S.; Pepe, F. R.; Hegedus, C. R. *J. Coat. Technol. Res.* **2008**, *5*, 233.

27. Rashvand, M.; Ranjbar, Z.; Rastegar, S. *Prog. Org. Coat.* **2011**, *71*, 362.

28. Hong, J. I.; Winberg, P.; Schadler, L. S.; Siegel, R. W. *Mater. Lett.* **2005**, *59*, 473.

29. Jiao, C.; Zhuo, J.; Chen, X. *Plast. Rubber Compos.* **2013**, *42*, 374.

30. Liu, L. M.; Qi, Z. N.; Zhu, X. G. *J. Appl. Polym. Sci.* **1999**, *71*, 1133.

31. Bhutto, A. A.; Vesely, D.; Gabrys, B. *J. Polymer* **2003**, *44*, 6627.

32. Chun, L.; Imae, T. *Macromolecules* **1994**, *37*, 2411.

33. Madejová, J.; Arvaiová, B.; Komadel, P. *Spectrochim. Acta Part A* **1999**, *55*, 2467.

34. Li, B.; Wang, Y. *Superlatt. Microstruct.* **2010**, *47*, 615.

35. Liu, Z. L.; Deng, J. C.; Deng, J. J.; Li, F. F. *Mater. Sci. Eng. B* **2008**, *150*, 99.

36. Wang, J. X.; Sun, X. W.; Yang, Y.; Akyaw, K. K.; Huang, X. Y.; Yin, J. Z.; Wei, J.; Demir, H. V. *Nanotechnology* **2011**, *22*, 325704.

37. Tang, L. C.; Wang, X.; Gong, L. X.; Peng, K.; Zhao, L.; Chen, Q.; Wu, L. B.; Jiang, J. X.; Lai, G. Q. *Compos. Sci. Technol.* **2014**, *91*, 63.

38. Tang, L. C.; Wan, Y. J.; Yan, D.; Pei, Y. B.; Zhao, L.; Li, Y. B.; Wu, L. B.; Jiang, J. X.; Lai, G. Q. *Carbon* **2013**, *60*, 16.

39. Guo, S. Z.; Zhang, C.; Peng, H. D.; Wang, W. Z.; Liu, T. X. *Compos. Sci. Tech.* **2011**, *49*, 791.

40. Bourbigot, S.; Le Bras, M.; Delobel, R.; Breant, P.; Tremillon, J. *Carbon* **1995**, *33*, 283.

41. Jiao, C. M.; Chen, X. L. *J. Therm. Anal. Calorim.* **2009**, *98*, 813.